

The Black Hole Binary Nova Scorpii 1994 (GRO J1655-40): An improved chemical analysis[★]

J. I. González Hernández^{1,2,3}, R. Rebolo^{3,4}, and G. Israelian³

¹ Observatoire de Paris-Meudon, GEPI, 5 place Jules Janssen, 92195 Meudon Cedex, France
e-mail: Jonay.Gonzalez-Hernandez@obspm.fr

² CIFIST Marie Curie Excellence Team

³ Instituto de Astrofísica de Canarias, E-38205 La Laguna, Tenerife, Spain
e-mail: rrl@iac.es, gil@iac.es

⁴ Consejo Superior de Investigaciones Científicas, Spain

Received January, 2007; accepted –

ABSTRACT

Context. The chemical analysis of secondary stars of low mass X-ray binaries provides an opportunity to study the formation processes of compact objects, either black holes or neutron stars.

Aims. Following the discovery of overabundances of α -elements in the Keck I/HIRES spectrum of the secondary star of Nova Scorpii 1994 (Israelian et al. 1999), we obtained VLT/UVES high-resolution spectroscopy with the aim of performing a detailed abundance analysis of this secondary star.

Methods. Using a χ^2 -minimization procedure and a grid of synthetic spectra, we derive the stellar parameters and atmospheric abundances of O, Mg, Al, Ca, Ti, Fe and Ni, using a new UVES spectrum and the HIRES spectrum.

Results. The abundances of Al, Ca, Ti, Fe and Ni seem to be consistent with solar values, whereas Na, and especially O, Mg, Si and S are significantly enhanced in comparison with Galactic trends of these elements. A comparison with spherically and non-spherically symmetric supernova explosion models may provide stringent constraints to the model parameters as mass-cut and the explosion energy, in particular from the relative abundances of Si, S, Ca, Ti, Fe and Ni.

Conclusions. Most probably the black hole in this system formed in a hypernova explosion of a 30–35 M_{\odot} progenitor star with a mass-cut in the range 2–3.5 M_{\odot} . However, these models produce abundances of Al and Na almost ten times higher than the observed values.

Key words. black holes physics–stars:abundances–stars:individual (Nova Scorpii 1994, GRO J1655-40)–supernovae: general–X-rays: binaries

1. Introduction

The low mass X-ray binary Nova Scorpii 1994 (GRO J1655–40) is one of the black hole transients that has attracted more attention in the last decade. It was discovered on 1994 July 27 with BATSE on board the *Compton Gamma Ray Observatory* (Zhang et al. 1994). The strong evidence that the compact object is a black hole was presented by Bailyn et al. (1995) who suggested a mass function of $f(M) = 3.16 \pm 0.15 M_{\odot}$. A self-consistent analysis of the ellipsoidal light curves of the system has yielded masses of 5.4 ± 0.3 and $1.45 \pm 0.35 M_{\odot}$ for the black hole and the companion star (Beer & Podsiadlowski 2002).

Israelian et al. (1999) found evidence of the formation of the black hole in an explosive supernova (SN) event. Using a high-resolution spectrum obtained with the Keck I Telescope, they found that the atmosphere of the secondary was enriched by a factor of 6–10 in several α -process elements (O, Mg, Si and S). These elements, almost exclusively synthesized during supernova explosions, cannot be produced in a low-mass secondary star which must have been exposed to the supernova material ejected when the compact remnant was formed. Subsequent dis-

cussions on the large amount of S, O, Mg and Si have considered this object as a relic of a hypernova and Gamma Ray Burst (Brown et al. 2000). More recently, these abundance anomalies were compared with a variety of SN models, including standard as well as hypernova models (for several progenitor masses and geometries), and a simple model of the evolution of the binary and the pollution of the secondary (Podsiadlowski et al. 2002). The observed anomalies were explained for a large range of model parameters, providing substantial fallback and mixing between the fallback matter and the ejecta.

Mirabel et al. (2002) found additional independent evidence that the black hole in this system formed in a SN explosion. They determined the proper motion of the system using the *Hubble Space Telescope* (HST) and computed its galactocentric orbit. The system moves with a runaway velocity of $\sim 112 \pm 18$ km s⁻¹ in a highly eccentric galactic orbit.

Here we improve the chemical analysis of the secondary star including more elements like Na, Al, Ca, Ni and Li and refining the abundance measurements of elements already studied by Israelian et al. (1999).

Send offprint requests to: J. I. González Hernández

[★] Based on observations obtained with UVES at VLT Kueyen 8.2 m telescope in programme 073.D-0473(A)

2. Observations

We obtained 14 spectra of Nova Sco 94 with the UV-Visual Echelle Spectrograph (UVES) at the European Southern Observatory (ESO), *Observatorio Cerro Paranal*, using the 8.2 m Very Large Telescope (VLT) on 2000 April 16 and 2000 June 18, covering the spectral regions $\lambda\lambda 3300\text{--}4500\text{ \AA}$, $\lambda\lambda 4800\text{--}5800\text{ \AA}$ and $\lambda\lambda 5800\text{--}6800\text{ \AA}$ at resolving power $\lambda/\delta\lambda \sim 43,000$. The total exposure time was 5.6 hours. The spectra were reduced in a standard manner using the UVES reduction package within the MIDAS environment. In this paper, we will also make use of one spectrum taken with the HIRES spectrograph at Keck telescope, covering the spectral region $\lambda\lambda 6800\text{--}8800\text{ \AA}$, previously used by Israelian et al. (1999). This near-IR spectrum has been boxcar-smoothed in wavelength with steps of 0.3 \AA , providing a $S/N \sim 45\text{--}50$ in the continuum.

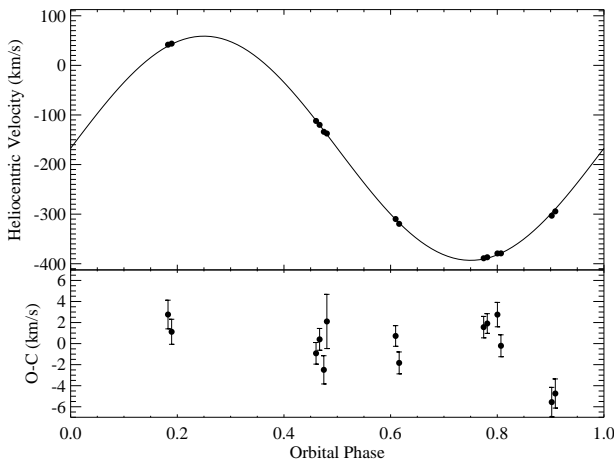


Fig. 1. Radial velocities of Nova Scorpii 1994 folded on the orbital solution of the data with best fitting sinusoid. Individual velocity errors are $\leq 1.5\text{ km s}^{-1}$ and are not plotted because they are always smaller than the symbol size. The bottom panel shows the residuals of the fit.

2.1. Revised orbital parameters

We extracted the radial velocities by cross-correlating each UVES spectrum of the target with the spectrum of a F6IV template star (Shahbaz et al. 1999) taken from S⁴N database (HIP 46853, Allende Prieto et al. 2004), using the software MOLLY developed by T. R. Marsh. A χ^2 sine wave fit to the obtained velocities yields to the following orbital solution (see Fig. 1): $\gamma = -167.1 \pm 0.6\text{ km s}^{-1}$, $K_2 = 226.1 \pm 0.8\text{ km s}^{-1}$, $P = 2.62120 \pm 0.00014\text{ d}$, and $T_0 = 2453110.5637 \pm 0.0019\text{ d}$, where T_0 is defined as the corresponding time of the closest inferior conjunction of the companion star, and the quoted uncertainties are at 1σ . This orbital period, P , together with the velocity amplitude of the orbital motion of the secondary star, K_2 , leads to a mass function of $f(M) = 3.16 \pm 0.03\text{ M}_\odot$, consistent with previous results (Bailyn et al. 1995; Orosz & Bailyn 1997).

The derived radial velocity of the center of mass of the system disagrees somewhat (at the 3σ level) with previous studies ($\gamma = -150 \pm 19\text{ km s}^{-1}$, Bailyn et al. 1995; $\gamma = -142.4 \pm 1.6\text{ km s}^{-1}$, Orosz & Bailyn 1997; $\gamma = -141.9 \pm 1.3\text{ km s}^{-1}$, Shahbaz et al. 1999). Note that our high-resolution data has a factor

greater than 5 better spectral resolution than the data these authors used. However, Shahbaz et al. (1999) estimate the uncertainty in their individual radial velocity measurements at typically 6 km s^{-1} , whereas our individual measurements have error bars of roughly 1 km s^{-1} . In addition, we have checked the accuracy of the wavelength calibration using the $\lambda 6300.2\text{ [O I]}$ sky line but unfortunately, its line profile appears distorted in each individual spectra of the target probably due to stellar lines, providing an estimate of its line center within 3 km s^{-1} . These uncertainties seem not to be enough to explain the difference between both radial velocity measurements.

2.2. Secondary spectrum

The individual UVES spectra were corrected for radial velocity and combined in order to improve the signal-to-noise ratio. After binning in wavelength with steps of 0.3 \AA the final UVES spectrum had a signal-to-noise ratio of 120–150 in the continuum in the red part of the spectrum. This spectrum is displayed in Fig. 2. Following Marsh et al. (1994), we computed the optimal $v \sin i$ by subtracting broadened versions of a template star (HIP 46583), in steps of 1 km s^{-1} , and minimizing the residual. We used an spherical rotational profile with linearized limb-darkening $\epsilon = 0.55$ (Al-Naimiy 1978). The best fit corresponds to a $v \sin i = 87^{+8}_{-4}\text{ km s}^{-1}$, where the errors have been derived by assuming extreme cases for $\epsilon = 0 - 1$. These values are consistent with previous studies ($v \sin i = 86^{+3.3}_{-3.6}\text{ km s}^{-1}$, Shahbaz et al. 1999). Our derived rotational velocity, combined with our value of the velocity amplitude, K_2 , implies a binary mass ratio $q = 0.329 \pm 0.047$. Shahbaz (2003) might have determined a more accurate value of the mass ratio, $q = 0.419 \pm 0.028$, by comparing synthetic spectra, which incorporate the secondary's Roche geometry, with an intermediate resolution spectrum of Nova Sco 94.

2.3. Diffuse interstellar bands

We obtained the spectrum of the interstellar medium (ISM) from our own observations. Due to the radial velocity of each individual exposure, in the average spectrum of all the individual spectra, the interstellar medium features are smoothed out. We subtracted the stellar features in each individual spectrum and combined them to obtain a spectrum that contains the ISM features. We tentatively identified in this spectrum 31 diffuse interstellar bands with equivalent widths typically in the range $10\text{--}65\text{ m\AA}$, although there are strong ISM features at $6060, 6202, 6283$ and 6613 \AA with equivalent widths of $148, 207, 555$ and 175 m\AA , respectively (Galazutdinov et al. 2000). In addition, the Na doublet at 5889 and 5895 \AA show equivalent width of 1.124 and 1.006 \AA . We took care that these bands did not affect the lines selected for the chemical analysis described in the next section.

3. Chemical Analysis

3.1. Stellar Parameters

In the normalized spectra of X-ray transients, although observed at quiescence, the stellar lines of the secondary star may be veiled by the flux coming from the accretion disc. This effect is more relevant in secondary stars of low luminosity. In the optical range, this veiling appears to drop toward longer wavelengths (e.g. Marsh et al. 1994). In our analysis, we tried to infer the stellar atmospheric parameters of the secondary star, using a tech-

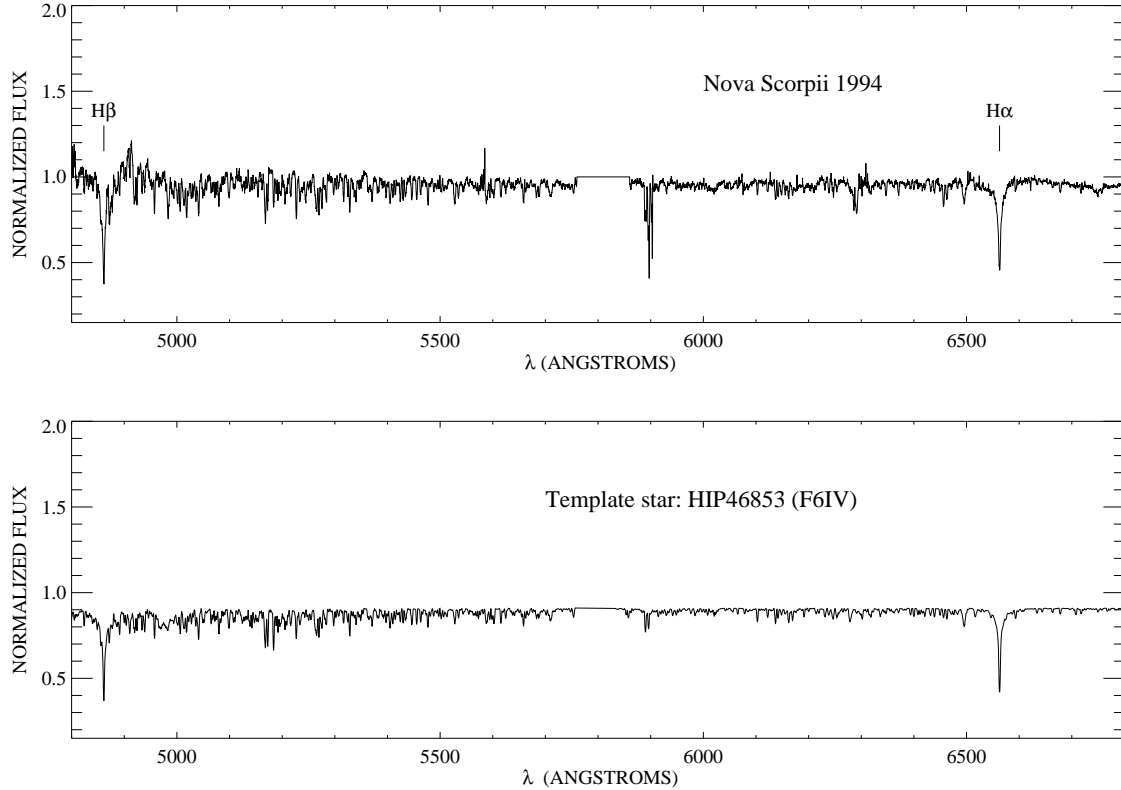


Fig. 2. Observed spectrum of the secondary star of Nova Scorpii 1994 (top) and of a properly broadened template (HIP 46583, bottom).

nique which compares a grid of synthetic spectra with the observed VLT/UVES spectrum, via a χ^2 -minimization procedure. This procedure takes into account the effect that veiling causes on the stellar lines and it has been applied in other X-ray binaries (A0620-00, González Hernández et al. 2004; Centaurus X-4, 2005; and XTE J1118+480, 2006). For Nova Sco 94, we have also considered any possible veiling from the accretion disc.

For this purpose, we firstly identified moderately strong and relatively unblended lines of the elements of interest in the high resolution solar atlas of Kurucz et al. (1984). We compute synthetic spectra with the local thermodynamic equilibrium (LTE) code MOOG (Snedden 1973), adopting the atomic line data from the Vienna Atomic Line Database (VALD, Piskunov et al. 1995) and using a grid of LTE model atmospheres (Kurucz 1993). We adjusted the oscillator strengths of the selected lines until reproducing both the solar atlas of Kurucz et al. (1984) with solar abundances (Grevesse et al. 1996) and the spectrum of Procyon with its derived abundances (Andrievsky et al. 1995). The changes we applied to the $\log gf$ values taken from VALD database are $\Delta \log gf \lesssim 0.2$ dex. However, in some cases, we modified the $\log gf$ values even in the range 0.2–0.4 dex for some lines as for instance, the O I $\lambda 6156$ – 8 \AA lines and the Mg I $\lambda 5528 \text{ \AA}$ and $\lambda 6318$ – 9 \AA lines (see Tables 2 and 3).

We selected six spectral features containing in total 42 lines of Fe I with excitation potentials between 1 and 5 eV. We generated a grid of synthetic spectra for these features varying as free parameters, the star effective temperature (T_{eff}), the surface gravity ($\log g$), the metallicity ($[\text{Fe}/\text{H}]$), and the veiling from the accretion disc, which was assumed to be a linear function of wavelength, and thus characterized by two parameters, its value at 4500 \AA , $f_{4500} = F_{\text{disc}}^{4500}/F_{\text{sec}}^{4500}$, and the slope, m_0 . Note that the total flux is defined as $F_{\text{total}} = F_{\text{disc}} + F_{\text{sec}}$, where F_{disc} and

Table 1. Ranges and steps of model parameters

Parameter	Range	Step
T_{eff}	5500 \rightarrow 7500 K	100 K
$\log(g/\text{cm s}^2)$	3. \rightarrow 5	0.1
$[\text{Fe}/\text{H}]$	-0.5 \rightarrow 1	0.05
f_{4500}	0 \rightarrow 0.6	0.05
m_0	0 \rightarrow -0.00027	-0.00003

F_{sec} are the flux contributions of the disc and the continuum of the secondary star, respectively. The microturbulence, ξ , was fixed in each atmospheric model according to the calibration as a function of effective temperature and surface gravity reported by Allende Prieto et al. (2004). Such calibration has been derived for stars of the solar neighbourhood with similar metallicity as the secondary star in Nova Sco 94. For the stellar parameters of the secondary star, determined below, this calibration provides a microturbulence of $\xi = 1.9 \text{ km s}^{-1}$.

The five free parameters were varying using the ranges and steps given in Table 1. In Fig. 3 we show the resulting histograms of these parameters corresponding to 1000 realizations of observed spectrum. We have not found any clear evidence of veiling from the accretion disc in the spectral region analysed ($\lambda 5400$ – 6800 \AA), as expected for the spectral type of the secondary star. The comparison of this grid, using a bootstrap Monte-Carlo method, gives the most likely values $T_{\text{eff}} = 6100 \pm 200 \text{ K}$, $\log(g/\text{cm s}^2) = 3.7 \pm 0.2$, $[\text{Fe}/\text{H}] = -0.1 \pm 0.1$, $f_{4500} = 0.15 \pm 0.05$, and $m_0 = -0.00012 \pm 0.00003$. This metallicity determination is consistent with the values reported

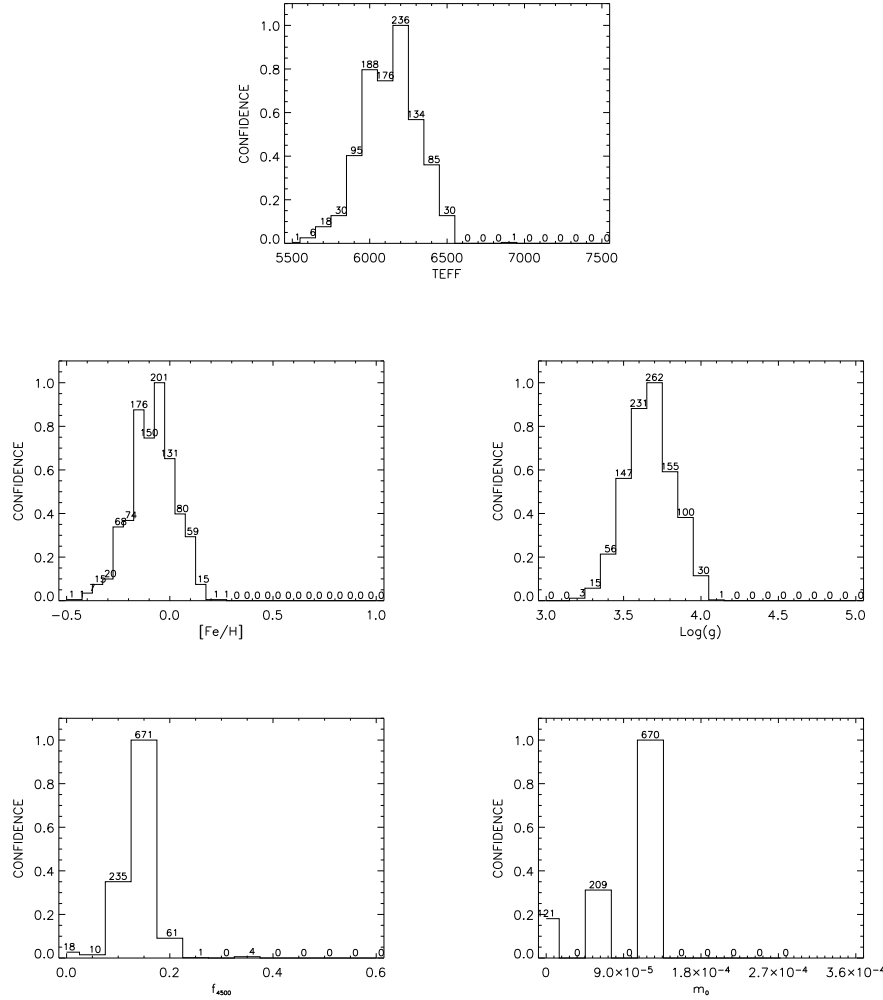


Fig. 3. Distributions obtained for each parameter using Monte Carlo simulations. The labels at the top of each bin indicate the number of simulations consistent with the bin value. The total number of simulations was 1000.

in the literature ($[\text{Fe}/\text{H}] = 0.1 \pm 0.2$, Israelian et al. 1999; $[\text{Fe}/\text{H}] = -0.1 \pm 0.15$, Buxton & Vennes 2001), whereas the effective temperature is slightly lower than the values obtained by these authors ($T_{\text{eff}} = 6400 \pm 250$ K, Israelian et al. 1999; $T_{\text{eff}} = 6500 \pm 50$ K, Buxton & Vennes 2001), although consistent within the error bars. We should remark that these authors used a different approach to derive the stellar parameters. Israelian et al. (1999) adopted the stellar parameters from previous calibrations of the spectral type and luminosity classification of the secondary star as a F6III/F7IV star. On the other hand, Buxton & Vennes (2001) determined the effective temperature by fitting a lower quality spectrum, in particular, the wings of H_α profile.

3.2. Stellar abundances

We inspected several spectral regions in both VLT/UVES and Keck I/HIRES spectra, searching for suitable lines for a detailed chemical analysis. Using the derived stellar parameters, we firstly determined the Fe abundance from each individual feature in the observed UVES spectrum (see Table 2). Since we knew of a potential enhancement of α -elements in the atmosphere of this star (Israelian et al. 1999), we computed new LTE model atmospheres with α -elements enhanced by +0.4 dex with respect to solar using the Linux version (Sbordone et al. 2004)

of the ATLAS code (Kurucz 1993). We used the new Opacity Distribution Functions (ODFs) of Castelli & Kurucz (2003) with the corresponding metallicity of the secondary star. In Fig. 4 we show some of the spectral regions analysed to obtain the Fe abundance. This figure also shows the best synthetic spectral fit to the observed spectrum of a template star (HIP 46853 with $T_{\text{eff}} = 6310$ K, $\log g = 3.91$ and $[\text{Fe}/\text{H}] = -0.08$ dex) using the stellar parameters and abundances determined by Allende-Prieto et al. (2004). Thus, we only use as abundance indicators those features which were well reproduced in the template star. The chemical analysis is summarized in Table 4. For the elements O, Mg, S, Si, Ti, previously studied by Israelian et al. (1999), we selected the most suitable lines in the UVES and HIRES spectra, whereas for other elements Na, Al, Ca, Ni, Fe and Li, we only used spectral features in the VLT/UVES spectrum. In Table 4 we provide the average abundance of each element extracted from the analysis of several features. The number of features analysed for each element is also stated. Individual element abundances derived from each feature are given in Table 2 and Table 3. The errors on the element abundances show their sensitivity to the uncertainties on the effective temperature, ΔT_{eff} , surface gravity, $\Delta \log g$, and the dispersion of the measurements from different spectral features, $\Delta \sigma$. The errors $\Delta \sigma$ were estimated as $\Delta \sigma = \sigma / \sqrt{N}$, where σ is the standard deviation of

Table 2. Adopted $\log gf$ values of important lines in the VLT/UVES spectrum. This line list do not included the weaker lines which these lines are blended with. The best fit abundance computed in LTE, $[X/H]$, is also given for each feature.

Species	λ (Å)	χ (eV)	$\log gf$	[X/H]	Species	λ (Å)	χ (eV)	$\log gf$	[X/H]
Fe I	5462.970	4.473	-0.15	–	Si I	6748.682	7.868	-0.80	–
Fe I	5463.276	4.434	0.11	-0.20	Si I	6748.837	7.868	-0.60	0.70
Fe I	5466.396	4.371	-0.63	–	Si I	6757.007	7.870	-0.90	–
Fe II	5534.847	3.245	-2.76	–	Si I	6757.171	7.870	-0.31	0.55
Fe I	5535.418	4.186	-0.96	0.15	Si I	5675.417	5.619	-1.23	0.25
Fe I	5554.895	4.548	-0.39	-0.20	Si I	5675.756	5.619	-2.08	–
Fe I	5615.644	3.332	0.05	-0.20	Si I	5684.484	4.954	-1.70	0.60
Fe I	6191.558	2.433	-1.52	-0.10	Si I	6112.928	5.616	-2.25	0.75
Fe I	6230.723	2.559	-1.28	-0.10	Si I	6113.120	5.616	-2.58	–
Fe I	6393.610	2.433	-1.51	-0.10	Si I	6131.565	5.616	-1.70	0.25
Fe I	6400.001	3.602	-0.41	-0.20	Si I	6131.855	5.616	-1.70	–
Fe I	6592.914	2.727	-1.67	-0.05	Si I	6142.204	5.619	-2.50	–
Ca I	6102.723	1.879	-0.67	-0.25	Si I	6142.483	5.619	-1.55	0.50
Ca I	6122.220	1.886	-0.01	0.10	Si I	6145.016	5.616	-1.42	–
Ca I	6161.297	2.523	-1.35	-0.25	Si I	6155.150	5.619	-0.82	0.35
Ca I	6162.180	1.899	0.37	–	Si I	6155.693	5.619	-2.22	–
Ca I	6169.042	2.523	-0.78	0.05	Si I	6237.319	5.614	-1.15	0.70
Ca I	6169.563	2.526	-0.45	–	Si I	6238.286	5.082	-2.38	–
Ca I	6439.075	2.526	0.39	0.00	Si I	6331.956	5.082	-2.40	0.85
Ca I	6471.662	2.526	-0.71	0.15	Si I	6433.457	5.964	-1.62	0.90
Ca I	6475.236	4.131	-1.22	-0.35	Si I	6721.848	5.863	-1.17	0.70
Ca I	6717.685	2.709	-0.62	–	Ti I	5953.160	1.887	-0.52	0.20
Mg I	5167.321	4.346	-0.62	0.30	Na I	5682.633	2.102	-0.69	0.70
Mg I	5172.684	5.108	-1.99	0.00	Na I	5688.207	2.104	-0.25	0.55
Mg I	5183.604	5.108	-2.25	0.00	Na I	6154.226	2.102	-1.68	0.05
Mg I	5528.405	4.346	-0.62	0.60	Na I	6159.482	2.104	-1.36	-0.05
Mg I	6318.717	5.108	-1.99	0.30	Al I	6696.023	3.143	-1.83	0.05
Mg I	6319.237	5.108	-2.25	–	Al I	6696.185	4.022	-1.83	–
Mg I	6319.495	5.108	-2.43	–	Al I	6696.788	4.022	-1.85	–
O I	6155.966	10.740	-1.01	–	Al I	6698.673	3.143	-1.87	–
O I	6156.756	10.741	-0.89	–	Ni I	5475.425	3.833	-1.95	–
O I	6156.776	10.741	-0.69	0.90	Ni I	5476.900	1.826	-0.89	0.35
O I	6158.176	10.741	-1.00	–	Ni I	5625.312	4.089	-0.70	0.10
O I	6158.186	10.741	-0.41	–	Ni I	5628.335	4.089	-1.27	0.00
O I	6300.230	0.000	-9.81	–	Ni I	6116.199	4.089	-0.68	0.45
Si I	6743.440	7.866	-1.27	–	Ni I	6116.199	4.266	-0.82	–
Si I	6743.531	7.866	-0.92	0.50	Ni I	6118.094	4.088	-2.32	–
Si I	6743.640	7.866	-1.03	–	Ni I	6191.171	1.676	-2.55	-0.10
Si I	6748.573	7.868	-1.39	–					

Table 3. Same as Table 2 but for the important lines in the Keck I/HIRES spectrum.

Species	λ (Å)	χ (eV)	$\log gf$	[X/H]	Species	λ (Å)	χ (eV)	$\log gf$	[X/H]
Mg I	7875.434	5.932	-2.13	–	O I	7775.400	9.110	0.10	–
Mg II	7877.054	9.996	0.39	0.75	O I	8446.249	9.521	-0.46	–
Mg I	7877.478	5.932	-1.95	–	O I	8446.359	9.521	0.23	1.80
Mg I	7881.669	5.933	-1.51	0.70	O I	8446.759	9.521	0.01	–
Mg I	8712.676	5.932	-1.67	–	Si I	8693.137	7.870	-1.37	–
Mg I	8712.689	5.932	-1.37	0.60	Si I	8693.931	7.870	-0.51	0.90
Mg I	8717.803	5.933	-2.85	–	Si I	8694.626	7.870	0.08	–
Mg I	8717.816	5.933	-1.85	–	Si I	8646.371	6.206	-1.94	–
Mg I	8717.825	5.933	-0.93	0.65	Si I	8648.465	6.206	-0.30	0.55
Mg I	8736.006	5.946	-1.93	–	Si I	8728.010	6.181	-0.61	0.60
Mg I	8736.019	5.946	-0.69	0.65	Si I	8728.594	6.181	-1.72	–
Mg I	8736.019	5.946	-1.97	–	Si I	8729.282	6.181	-2.30	–
Mg I	8736.029	5.946	-1.02	–	Ti I	8434.957	0.848	-0.88	0.35
O I	7771.960	9.110	0.45	2.00	Ti I	8435.652	0.836	-1.02	–
O I	7774.180	9.110	0.31	–	Ti I	8438.923	2.256	-0.79	–

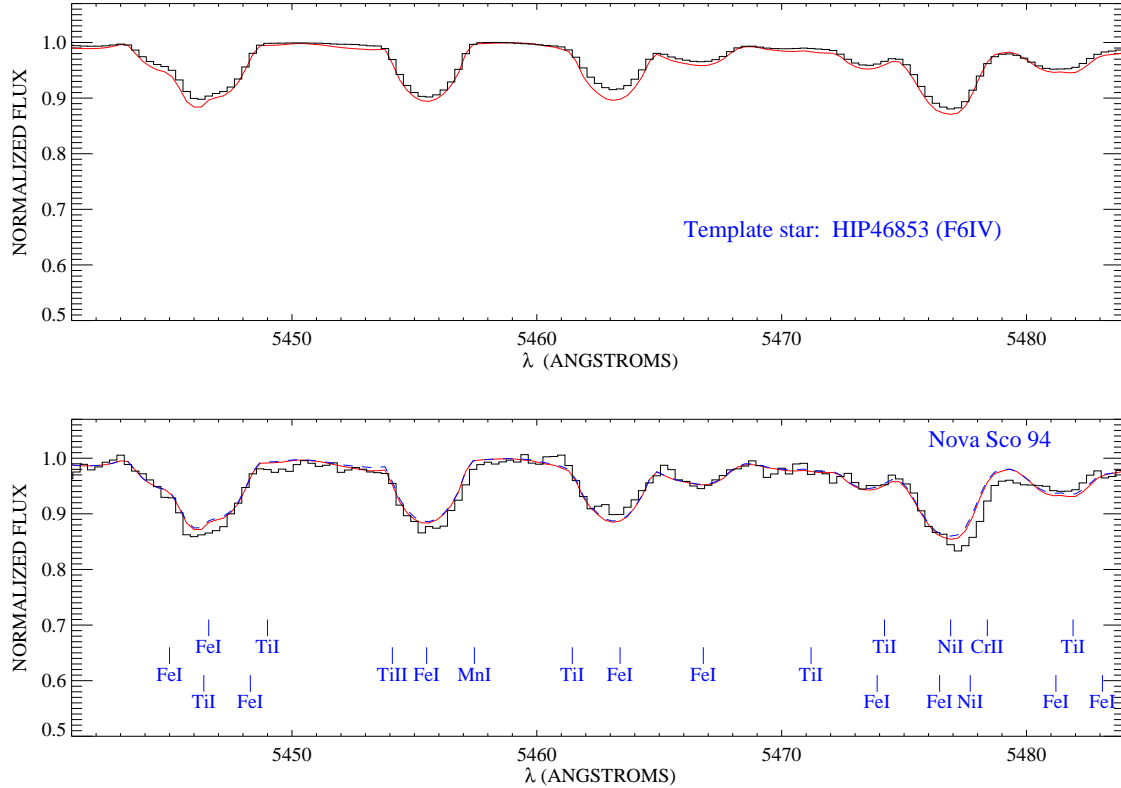


Fig. 4. Best synthetic spectral fits to the UVES spectrum of the secondary star in the Nova Scorpii 1994 system (bottom panel) and the same for a template star (properly broadened) shown for comparison (top panel). Synthetic spectra are computed for solar abundance ratios ($[E/Fe] = 0$ with $[Fe/H] = -0.1$, dashed line) and best fit abundance (solid line).

the N measurements. The errors $\Delta_{T_{\text{eff}}}$ and $\Delta_{\log g}$ were determined as $\Delta_{T_{\text{eff}}} = (\sum_{i=1}^N \Delta_{T_{\text{eff},i}})/N$ and $\Delta_{\log g} = (\sum_{i=1}^N \Delta_{T_{\log g,i}})/N$. The Al and Li abundance were derived from one spectral line (see Fig. 8) and the error associated to the dispersion of the measurements, σ , was assumed to be the average dispersion of Fe, Ca and Ni abundances, and in this case, $\Delta_{\sigma} = \sigma$. The total error given in Table 4 was derived using the following expression:

$$\Delta_{\text{tot}} = \sqrt{\Delta_{\sigma}^2 + \Delta_{T_{\text{eff}}}^2 + \Delta_{\log g}^2}.$$

3.2.1. Oxygen

The atomic data for O I lines were adopted from Ecuivillon et al. (2006) where oscillator strengths were slightly modified in order to obtain a solar oxygen abundance of $\log \epsilon(\text{O})_{\odot} = 8.74$. In Fig. 5 we display one of the spectral regions analysed, where the forbidden line [O I] $\lambda 6300.2$ Å is present. Unfortunately, we found this line inconvenient to provide a reliable abundance: it is very weak at the effective temperature of the secondary star; it is blended with stronger lines of Si I $\lambda 6299.6$ Å and Fe I $\lambda 6301.5$ due to high rotational broadening of the star; and the strong narrow diffuse band (see the feature labelled DIB in Fig. 5) at 6283.8 Å makes it difficult to place properly the continuum. An oxygen abundance of $[O/H] \sim 0.9$ (solid line in Fig. 5) seems not to fit at all the [O I] feature which may be better reproduced using a solar abundance synthetic spectrum (dashed line in Fig. 5).

Thus, we determined the oxygen abundance from three features containing: O I $\lambda 6156-8$ Å lines, which appear severely blended with Si I, Ca I and Fe I lines, and the relatively isolated

O I $\lambda 7771-5$ Å and O I $\lambda 8446$ Å triplets. In the left-bottom panel of Fig. 6 we show the O I $\lambda 6156-8$ Å lines in the VLT spectrum of the target in comparison with several synthetic spectra in LTE. The best fit in LTE gives an oxygen abundance of $[O/H]_{\text{LTE}} \sim 0.9$. While LTE appears to be practically valid for the O I $\lambda 6156-8$ Å (Takeda et al. 2005), the O I $\lambda 7771-5$ Å and O I $\lambda 8446$ Å suffers appreciable non-LTE effects (Ecuivillon et al. 2006). The NLTE corrections¹ were kindly provided by N. Shchukina (private communication; Shchukina 1987; Ecuivillon et al. 2006). For the stellar parameters and oxygen abundance of the secondary star, NLTE corrections were estimated at -0.988 and -0.926 for the near-IR O I $\lambda 7771-5$ Å and O I $\lambda 8446$ Å triplets, respectively.

3.2.2. Magnesium

The abundance of magnesium was determined from 5 Mg I spectral features in the optical VLT/UVES spectrum, including the three features of the Mg Ib triplet at 5167-83 Å, 4 Mg I spectral features in the near-IR Keck I/HIRES spectrum, where Mg I lines are isolated or weakly blended with other lines, and a Mg II spectral feature at 7877 Å. In Fig. 5 and the right-bottom panel of Fig. 6, we show some of the Mg I features included in the abundance analysis. Note that the best fit synthetic spectra displayed in these figures show the best fit abundance of each feature instead of the average abundance of each element given in Table 4. We should remark that the location of the continuum near the near-IR lines, where the S/N ~ 50 , is less accurate, than that of

¹ $\Delta_{\text{NLTE}} = \log \epsilon(X)_{\text{NLTE}} - \log \epsilon(X)_{\text{LTE}}$

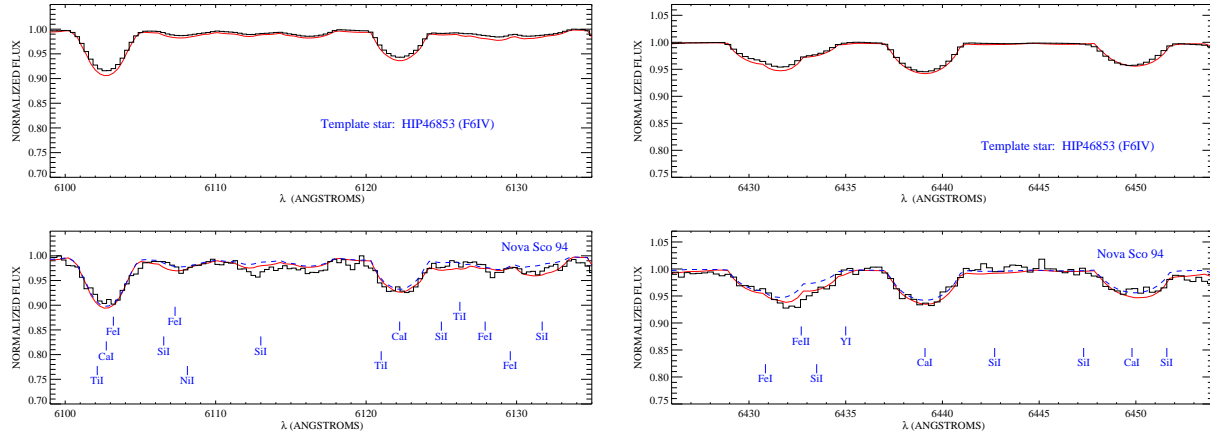


Fig. 7. The same as in Fig. 4, but for the spectral range $\lambda\lambda 6099\text{--}6135\text{ \AA}$ (left panels) and $\lambda\lambda 6426\text{--}6454\text{ \AA}$ (right panels).

Table 4. Chemical abundances of the secondary star in Nova Scorpii 1994

Element	$[X/H]_{\text{LTE}}^{\text{a,b}}$	σ	$\Delta_{\sigma}^{\text{c}}$	ΔT_{eff}	$\Delta \log g$	Δtot	$n_{\text{lines}}^{\text{d}}$
O ^e	0.91	0.07	0.04	0	0.07	0.09	3
Na	0.31	0.37	0.18	0.19	0	0.26	4
Mg	0.48	0.29	0.09	0.10	-0.03	0.15	10
Al	0.05	0.15	0.15	0.1	0	0.18	1
Si	0.58	0.21	0.06	0.05	0.01	0.08	12
S	0.66	0.18	0.09	-0.04	0.06	0.12	4
Ca	-0.02	0.17	0.07	0.12	0.01	0.14	7
Ti	0.27	0.11	0.07	0.2	0.05	0.22	2
Fe	-0.11	0.11	0.03	0.09	0.01	0.10	9
Ni	0	0.10	0.06	0.2	0.05	0.21	5
Li ^f	2.13	0.15	0.15	0.15	0	0.21	1

^a The solar element abundances were adopted from Grevesse et al. (1996) and Ecuivillon et al. (2006): $\log \epsilon(\text{O})_{\odot} = 8.74$, $\log \epsilon(\text{Na})_{\odot} = 6.33$, $\log \epsilon(\text{Mg})_{\odot} = 7.58$, $\log \epsilon(\text{Al})_{\odot} = 6.47$, $\log \epsilon(\text{Si})_{\odot} = 7.55$, $\log \epsilon(\text{S})_{\odot} = 7.21$, $\log \epsilon(\text{Ca})_{\odot} = 6.36$, $\log \epsilon(\text{Ti})_{\odot} = 4.99$, $\log \epsilon(\text{Fe})_{\odot} = 7.50$, $\log \epsilon(\text{Ni})_{\odot} = 6.25$

^b Element abundances (calculated assuming LTE) are $[X/H] = \log[N(X)/N(H)]_{\text{star}} - \log[N(X)/N(H)]_{\text{Sun}}$, where $N(X)$ is the number density of atoms. Uncertainties, Δtot , are at 1σ level and take into account the error in the stellar parameters and the dispersion of the measurements.

^c The errors from the dispersion of the best fits to different features, see text.

^d Number of features analysed for each element.

^e NLTE abundance of oxygen, see text.

^f Li abundance is expressed as:

$$\log \epsilon(\text{Li})_{\text{NLTE}} = \log[N(\text{Li})/N(\text{H})]_{\text{NLTE}} + 12$$

3.2.3. Silicon

The Si abundance was obtained from the 12 features with Si I lines often blended with other lines, some of them are displayed in Figs. 7 and 8. The dispersion of the abundance measurements from different lines is 0.2 dex, although the average abundance has a good accuracy due to the number of features analysed. As shown in Fig. 5, we found difficult to reproduce Si II lines, surprisingly strong in comparison with Si I lines, with the average Si abundance, so that, we decided not to consider them as abundance indicators. Shchukina & Trujillo Bueno (2001) pointed

out that NLTE effects for Si (with an ionization potential of 8.15 eV, slightly higher than that of Fe, 7.87 eV) would likely be similar to those found for Fe, which suffers from over-ionization, in a three-dimensional solar photospheric model. In addition, for species where over-ionization is prominent, the NLTE effects normally increase toward higher T_{eff} and lower $\log g$ (Asplund 2005).

Wedemeyer (2001) has performed a NLTE analysis of Si in the Sun and argued that most of the levels of Si I show almost negligible deviations from LTE, whereas Si II levels are overpopulated with respect to LTE. In particular, this author predicts NLTE corrections of -0.01 dex for one of the Si I lines we have analysed at 5684 Å. For the Si II lines at 6347 Å and 6371 Å the NLTE corrections are -0.097 dex and -0.064 dex for the Sun, respectively, and therefore 6 to 9 times higher for the Si II lines than for the Si I lines. These NLTE effects might be significantly larger for the Si II lines in the secondary star, giving rise to large NLTE corrections. The synthetic profile computed in NLTE would make stronger Si II lines, thus providing a better description of the observations. However, this conclusion must be clarified in forthcoming investigations. Note that, in fact, the synthetic spectral fits reproduce quite well the Si II features in the template, but these features are much stronger in the spectrum of the secondary star in Nova Sco 94.

3.2.4. Sulphur

In Fig. 8, we show another spectral region with the strong Si I $\lambda\lambda 6743\text{--}57\text{ \AA}$ lines. The overabundance of S is clearly seen in the spectrum of Nova Sco 94 when compared with the template. These three strong and unblended lines of sulphur clearly confirm the overabundance of sulphur in the secondary star of this system. We also included one S I feature at 8694 Å, found in the Keck spectrum, in the S abundance determination. Takeda-Hidai et al. (2002) and Takeda et al. (2005) have reported negligible corrections for S I $\lambda 8694\text{ \AA}$ lines. For the stellar parameters, metallicity and abundance ratio $[S/Fe] \sim +0.6$ dex of the secondary star, NLTE corrections are comprised in the range $-0.04 < \Delta_{\text{NLTE}} < -0.08$ dex. These corrections were not considered in the sulphur abundance given in Table 4, since they are almost negligible compared to the dispersion of the LTE abundances derived from different Si I lines. In addition, NLTE corrections for the S I $\lambda\lambda 6743\text{--}57\text{ \AA}$ lines are not available in the literature.

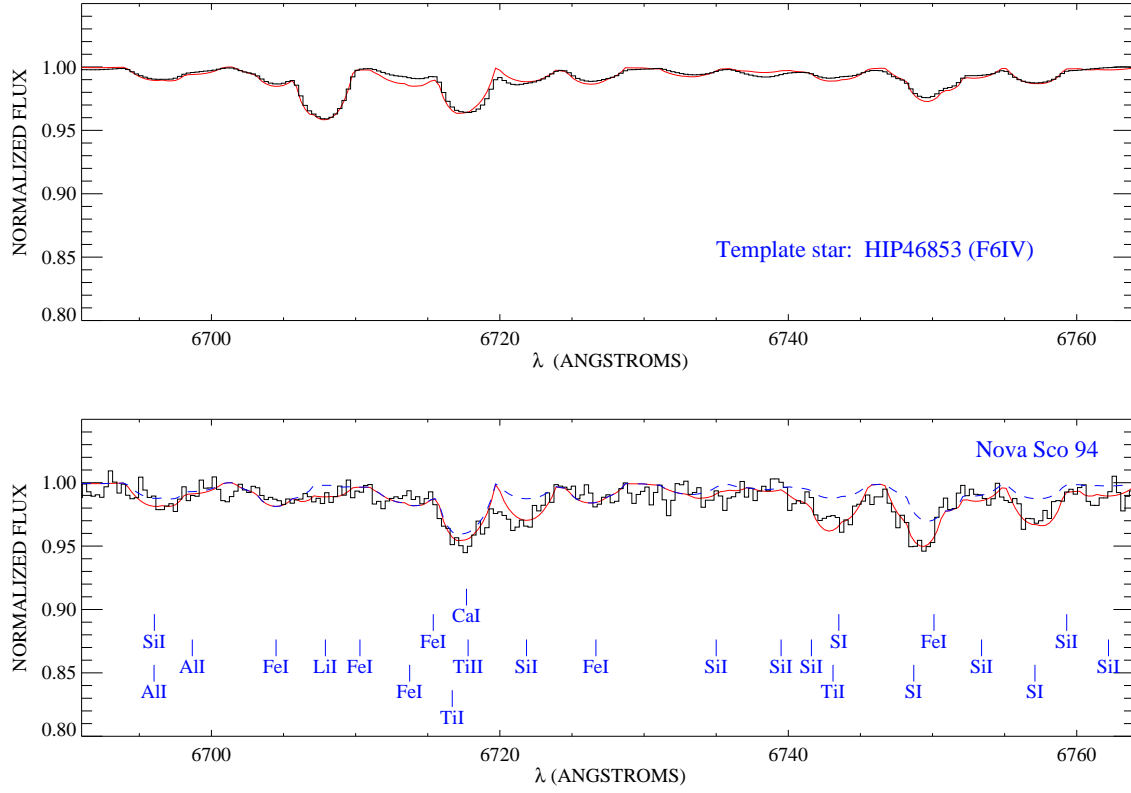


Fig. 8. The same as in Fig. 4, but for the spectral range $\lambda\lambda 6690\text{--}6760\text{ \AA}$.

3.2.5. Calcium

Calcium is one the α -elements that could not be measured in the analysis of the Keck spectrum reported in Israelian et al. (1999). The abundance of calcium was obtained from the analysis of 7 almost unblended and strong spectral features in the VLT spectrum. Some of these features are displayed in the left-bottom panel of Figs. 6, 7 and 8. NLTE abundance corrections have been reported for the Ca I $\lambda\lambda 6102, \lambda\lambda 6169, \lambda\lambda 6439$ and $\lambda\lambda 6471\text{ \AA}$ lines (Mashonkina et al. 2007), being $-0.05, -0.01, -0.13, -0.06$ dex, respectively for a model of $T_{\text{eff}} = 6000\text{ K}$ $\log g = 4$ dex and $[\text{Fe}/\text{H}] = 0$ dex. This results on an average correction $\Delta_{\text{NLTE}} < -0.05$ dex which does not have any significant impact on the Ca abundance.

3.2.6. Titanium

Israelian et al. (1999) could not measure a reliable abundance of Ti using the Keck spectra since they did not find spectral features with relatively unblended Ti I lines. Unfortunately, the signal-to-noise ratio in the spectral region from 5920 to 5960 \AA of the VLT/UVES spectrum of Nova Sco 94 where there are some Ti features is not enough to provide reliable abundances. This spectral region is close the edge of one of the arms of the UVES spectrograph. Thus, we finally selected one of these features in the VLT spectrum and another relatively unblended feature of Ti in the Keck spectrum. We emphasize that the Ti abundance must be considered with caution, although the UVES spectrum seems to indicate that Ti abundance is not as enhanced as other α -elements like O, Mg, Si and S, but it shows an abundance almost consistent with solar if we take into account the error bars (see Table 4).

3.2.7. The odd-Z elements: Na, Al

The Al I $\lambda\lambda 6696\text{--}8\text{ \AA}$ lines appear to be surprisingly weak since one could expect to obtain an overabundance of aluminum according to supernova yields (Umeda & Nomoto, 2002, 2005; Tominaga, Umeda & Nomoto 2007; Maeda et al. 2002). Baumüller & Gehren (1996, 1997) show that this doublet is not sensitive to NLTE conditions, with expected corrections $\Delta_{\text{NLTE}} < +0.05$ for models with similar stellar parameters as the secondary star.

The sodium abundance was determined from 4 features, typically blended with other lines (see Table 4). Its abundance is not as high as expected from yields of SN models which suggest a similar behaviour as aluminum. Baumüller et al. (1998) predict NLTE corrections $\Delta_{\text{NLTE}} < -0.03$ and $\Delta_{\text{NLTE}} < -0.05$ for the Al I $\lambda\lambda 5682\text{--}8$ and $\lambda\lambda 6154\text{--}60$ lines, respectively, which are not relevant in the abundance analysis.

3.2.8. Lithium

The best fit to the Li I $\lambda\lambda 6708\text{ \AA}$ feature provides an LTE abundance of $\log \epsilon(\text{Li})_{\text{LTE}} = 2.16 \pm 0.21$. We estimated the non-LTE abundance correction for this element, from the theoretical LTE and non-LTE curves of growth in Pavlenko & Magazzù (1996). We found $\Delta_{\text{NLTE}} = -0.03$. Due to the weakness of the absorption we consider this abundance estimate given in Table 2 as an upper limit².

According to the effective temperature of the secondary star ($T_{\text{eff}} = 6100 \pm 200\text{ K}$), slightly far from the *lithium gap* (between 6400 – 6800 K, Boesgaard & Tripicco 1986), this Li abundance

² The template star has $\log \epsilon(\text{Li})_{\text{LTE}} \sim 3.3$, which does not affect our results

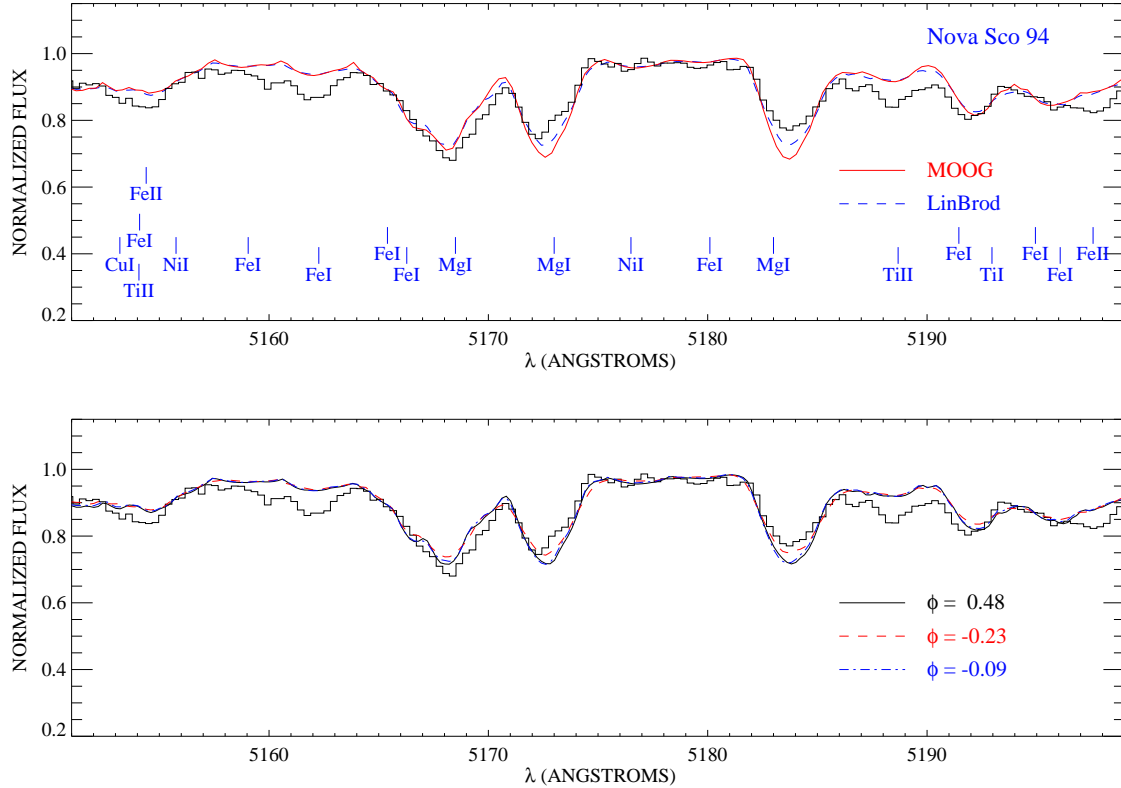


Fig. 9. Upper panel: Observed UVES spectrum of the secondary star in comparison with the average synthetic spectrum computed with LINBROD (dashed line) for all orbital phases and the synthetic spectrum computed with MOOG (solid line). An abundance of $[\text{Mg}/\text{H}] \sim 0.3$ dex has been adopted for all synthetic spectra. Bottom panel: Synthetic spectra computed with LINBROD for different orbital phases.

is consistent with that of main-sequence F type disc stars with ages in the range $\sim 1 - 3 \times 10^9$ yr with the similar metallicity (e.g. Boesgaard & Tripicco 1987; Balachandran 1991).

3.3. Comparison with the results of Foellmi et al.

In a recent paper, Foellmi, Dall & Depagne (2007) compared the results on the element abundances reported by Israelian et al. (1999) using the UVES spectra reported in this paper, taken in 2004, and additional VLT/UVES spectra taken in 2006. They confirm an enhanced oxygen abundance and a relatively low Ti and Ca abundance in the secondary star which is consistent with our results, but also claim that other α -elements do not show over-abundances in clear disagreement with our findings for Mg, Si and S. Their conclusions are based on equivalent widths of different spectral features as well as the comparison of synthetic spectra to the observed Mg Ib triplet at 5167–83 Å, the Si I triplet at 9228 Å and some other features of Mg I, Si I and S I in the spectral region from 8670 to 8740 Å.

We have revised the equivalent widths presented in Table 1 of Foellmi et al. (2007) in our VLT/UVES spectra obtained in 2004 and found slightly larger values which might be related to the continuum location. In addition, we find it confusing the system velocity of $\sim -88 \text{ km s}^{-1}$ reported by Foellmi et al. (2006) which they also used in Foellmi et al. (2007), in comparison with our value of $\sim -167 \text{ km s}^{-1}$ which is comparable to values previously reported in the literature. However, they obtained an orbital semiamplitude of $K_2 = 225 \pm 10 \text{ km s}^{-1}$ which is less accurate than our value, $K_2 = 226.1 \pm 0.8 \text{ km s}^{-1}$. Their larger error on the orbital semiamplitude could give rise to large errors

on the radial velocities applied to the individual spectra which might have slightly smoothed out the stellar lines in the average spectrum of the secondary star. This might explain why these authors found a rotational velocity of $v \sin i \sim 94 \text{ km s}^{-1}$ slightly larger than our value of $v \sin i \sim 87 \text{ km s}^{-1}$.

3.3.1. Sulphur

Foellmi et al. (2007) claim that sulphur is not enhanced in the secondary star. Indeed, we demonstrate in our paper that the sulphur features at 6743–57 Å are very well detected with $\text{S/N} \sim 150$ (as it is shown in Fig. 8 of this paper) and lead to a large overabundance of this element. The new features we are referring in our new paper basically confirm the sulphur overabundance in a completely independent way to Israelian et al. (1999). Foellmi et al. did not note these sulphur features in their paper which should be certainly present in the spectra they used. In addition, in Figs. 1 and 3 in Foellmi et al. (2007), the location of the continuum appears improperly low. The Si I features at 8693 and 9228 Å would lead to a larger abundance if the continuum is suitably placed. We should remark that due to the large rotational broadening of the secondary star, roughly 87 km s^{-1} , slight changes of the continuum location could give rise to considerably differences in the derived element abundances. The inspection of the lower panel of Fig. 1 in Foellmi et al. (2007) shows that the Fe I features, which are not expected to be enhanced, are not well reproduced by the synthetic spectrum because the continuum has been placed too low. After correction of the continuum in this figure, the Si I and Si I features at 8680 and 8694 Å would require higher abundances.

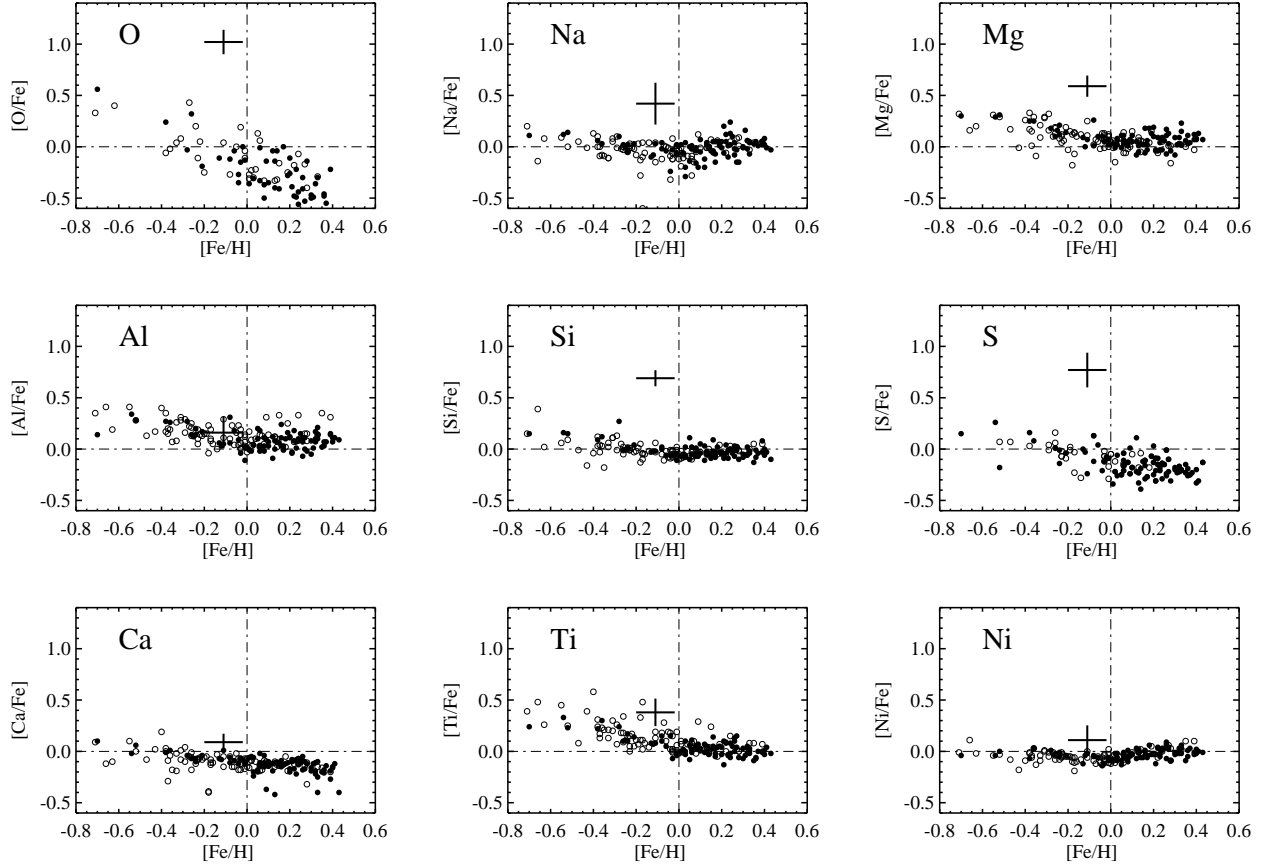


Fig. 11. Abundance ratios of the secondary star in Nova Scorpii 1994 (blue wide cross) in comparison with the abundances of G and K metal-rich dwarf stars. Galactic trends were taken from Ecuivillon et al. (2004), Ecuivillon et al. (2006) and Gilli et al. (2006). The size of the cross indicates the 1-sigma uncertainty. Filled and empty circles correspond to abundances for planet host stars and stars without known planet companions, respectively. For the abundance of oxygen in metal-rich dwarfs we have only considered abundance measurements in NLTE for the triplet O I 7771–5 Å. The dashed-dotted lines indicate solar abundance values.

average effective temperature of the star, which was assumed to be our spectroscopic estimate of the effective temperature, and the orbital parameters. We also adopted an orbital inclination of $\sim 69^\circ$ (Beer & Podsiadlowski 2002) and mass ratio of $q \sim 0.419$ (Shahbaz 2003). The code `LinBrod` divides the stellar surface in tiles, for which a local temperature and gravity is derived, uses the code `MOOG` to compute a synthetic spectrum for each tile, and finally integrates over the whole stellar surface. The average profile of Mg ib lines over all the observed orbital phases computed with `LinBrod` is weaker than the spherical profile computed with the code `MOOG` (see Fig. 9). The main reason of this difference is that the average surface gravity derived by `LinBrod`, which is shared by almost the 80 per cent of the tiles and only depends on the dynamical parameters, is $\log g = 3.5 \pm 0.1$, being lower than our estimate ($\log g = 3.7 \pm 0.2$) but marginally consistent within the error bars. The Mg ib lines at 5172 Å and 5183 Å become weaker for lower values of $\log g$. The Mg ib line at 5167 Å is blended with lines of other elements that have different sensitivity to changes of the stellar parameters and they somehow compensate the sensitivity of the Mg ib 5167 Å line. This figure also shows how the profile depends on the orbital phase, mostly due to the different velocity profile provided by the asymmetry of the stellar surface seen by the observer.

In Fig. 9, we adopted an abundance of $[\text{Mg}/\text{H}] \sim 0.3$ dex which is almost able to reproduce the observed features when the code `LinBrod` is used. Note that we have taken into account

a veiling factor of 7% estimated at this wavelength according to our determination of stellar and veiling parameters (see § 3.1). This abundance would be in agreement with the Mg i feature at 6319 Å which provides $[\text{Mg}/\text{H}] \sim 0.3$ using the code `MOOG` and is less sensitive to the surface gravity (see Table 2).

In Fig. 10 we displayed another spectral region where the S I 6743–57 Å are located. In this case, in contrast with the Mg ib lines, the synthetic spectrum computed with `LinBrod` is practically similar to that computed with `MOOG`, which indicates that these S I lines are not affected by the asymmetry of the stellar surface because they are hardly sensitive to the surface gravity. The Mg features analysed in the near-IR Keck spectrum are equally not affected because they are not sensitive to small variations of the stellar parameters and in addition, this spectrum was taken at an orbital phase close to 0, when the star looks almost spherical.

We should remark that in the average Mg abundance given in Table 4 we do not applied any correction to the Mg abundances derived from the Mg ib lines using the code `MOOG`, which are given in Table 2. The use of the program `LinBrod` would provide a slightly higher average Mg abundance and slightly smaller dispersion.

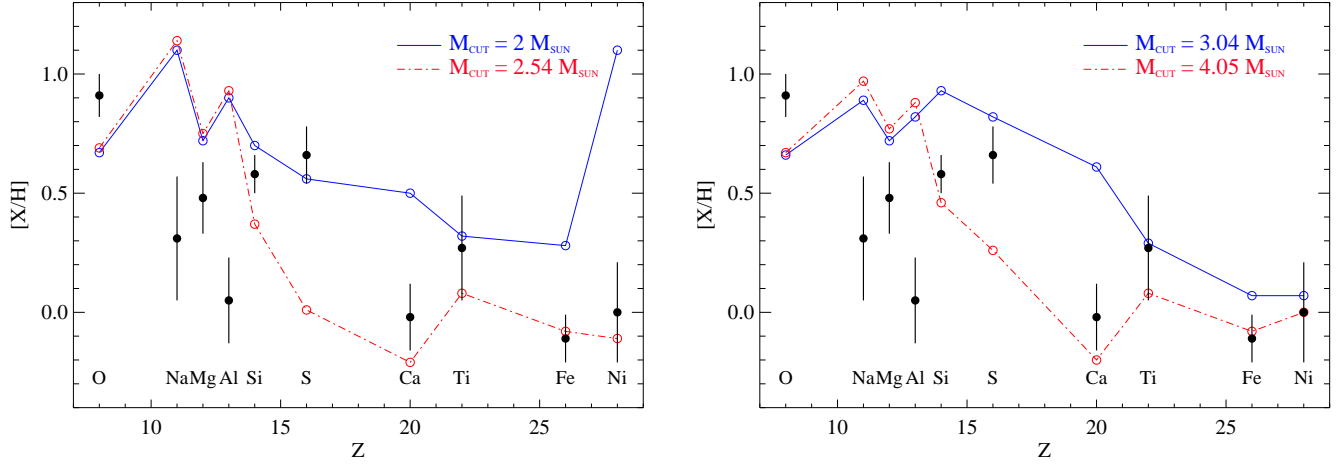


Fig. 12. Left panel: Observed abundances (filled circles with the error bars) in comparison with the expected abundances in the secondary star after having captured the 70% of the matter ejected within the solid angle subtended by the secondary from a spherically symmetric supernova explosion of kinetic energy $E_K = 10^{51}$ ergs for two different mass-cuts, $M_{\text{cut}} = 2 M_{\odot}$ (solid line with open circles), and $M_{\text{cut}} = 2.54 M_{\odot}$ (dashed-dotted line with open circles). Right panel: the same as left panel but for a spherically symmetric hypernova explosion of kinetic energy $E_K = 20 \times 10^{51}$ ergs for two different mass-cuts, $M_{\text{cut}} = 3.04 M_{\odot}$ (solid line with open circles), and $M_{\text{cut}} = 4.05 M_{\odot}$ (dashed-dotted line with open circles).

4. Discussion

4.1. Heavy elements

The abundances ratios of O, Mg, S, Si and Na with respect to Fe in the secondary star of Nova Sco 94 are considerably higher than those in stars of similar Fe content (see Fig. 11) while, on the contrary, Al, Ca, Ti and Ni seem to be consistent with the Galactic trends. As can be seen in Table 4, the uncertainties induced by effective temperature and gravity are considerably diminished when dealing with abundance ratios and the major source of error in $[X/\text{Fe}]$ is associated with the dispersion, Δ_{σ} , of abundances obtained from different features of the same element. Thus, the error bars of the abundance ratios displayed in Fig. 11 were estimated as:

$$(\Delta[X/\text{Fe}])^2 = \Delta_{\sigma, X}^2 + (\Delta_{T_{\text{eff}}, X} - \Delta_{T_{\text{eff}}, \text{Fe}})^2 + (\Delta_{\log g, X} - \Delta_{\log g, \text{Fe}})^2 + \Delta_{\sigma, \text{Fe}}^2$$

Podsiadlowski et al. (2002) showed that a relatively simple model of pollution of the secondary star from a supernova explosion can explain most of the observed α -element abundance enhancements in the secondary star.

Since we have extended the number of elements analysed in the secondary star, we will intend to extract more information on the SN explosion by comparing our new results with yields from current supernova models kindly provided by Umeda, Nomoto et al. (2002, 2005).

4.1.1. Spherical SN explosion

We have considered spherically symmetric supernova and hypernova models for a $30 M_{\odot}$ progenitor (8.5 He core, Umeda & Nomoto, 2002, 2005; Tominaga, Umeda & Nomoto 2007) and a $\sim 2 M_{\odot}$ secondary star, initially placed at an orbital distance of $\sim 10 R_{\odot}$ (after the binary orbit has been recircularized), which needs to capture almost 70% of the matter ejected within the solid angle subtended by the secondary as seen from the helium star to achieve the observed abundances. We adopted an initial black hole mass of $M_{\text{BH}, i} \sim 5 M_{\odot}$, before the secondary star begins to transfer matter onto the compact object. Note that the

dynamical estimate of the black hole mass provides $M_{\text{BH}, f} \sim 5.4 M_{\odot}$ (Beer & Podsiadlowski 2002). We have also assumed different mass-cuts (M_{cut} , the mass that initially collapsed forming the compact remnant) and all the fallback material (M_{fall} , amount of mass which is eventually accreted by the compact core) to be completely mixed with the ejecta. We have performed simulations of the expected abundances of the secondary star after capturing matter from the SN ejecta as in González Hernández et al. (2004). In our simulations we varied the mass-cut from 1.35 to $5.05 M_{\odot}$ in steps of ~ 0.5 and $1 M_{\odot}$ (depending on the mass bins given in the explosion models), and all the simulations keep $M_{\text{BH}, i} = M_{\text{cut}} + M_{\text{fall}}$. In addition, all the matter captured is completely mixed with the whole material of the secondary star. In Fig. 12 we show the observed abundances in comparison with the expected abundances for two different mass-cuts. The error bars in Fig. 12 correspond to the total errors given in Table 4. Note that some of the elements are highly sensitive to mass-cuts, for instance, the supernova model (left panel in Fig. 12) predicts a strong dependence of Ni, Ca and S abundances on the selected mass-cuts since the explosive burning is only able to create these elements at relatively deep layers in the explosion. It would be acceptable to find an agreement between the observed abundances and one of the two models displayed or at least to find the observed values in a middle location between both predictions. This comparison using both spherically symmetric supernova and hypernova models allow us to extract the following conclusions:

- The relatively low abundances of Ca, Ti, Ni and Fe may indicate that the mass-cut was in the range $2\text{--}3.5 M_{\odot}$ for explosion energies $(1 - 20) \times 10^{51}$ ergs.
- These explosion models suggest that the higher the energy the larger amounts of elements like S, Si, Ti and Ca, and even Fe and Ni are created. Thus, the substantial enhancement of Si and S in the secondary star favours higher explosion energies and hence, the hypernova scenario (Brown et al. 2000).
- In addition, even for higher energies, the amount of S decreases significantly above a mass-cut of $3.5 M_{\odot}$ confirming the need of efficient mixing processes between the fallback matter and the ejecta (Kifonidis et al. 2000).

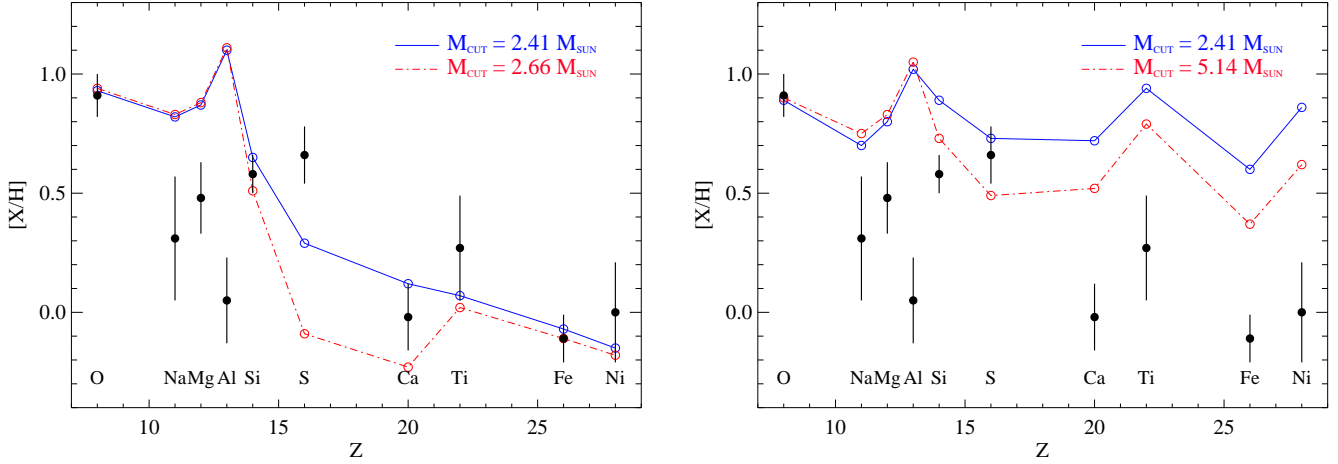


Fig. 13. Left panel: Observed abundances (filled circles with the error bars) in comparison with the expected abundances in the secondary star after having captured the 10% of the matter ejected within the solid angle subtended by the secondary from a non-spherically symmetric supernova explosion of kinetic energy $E_K = 10^{52}$ ergs for two different mass-cuts, $M_{\text{cut}} = 2.41 M_{\odot}$ (solid line with open circles), and $M_{\text{cut}} = 2.66 M_{\odot}$ (dashed-dotted line with open circles). This model corresponds to the matter ejected in the equatorial plane of the primary where we assumed that the secondary star is located (see more details in González Hernández et al. 2005b). Right panel: the same as left panel but in this model we have assumed complete lateral mixing where all the material within given velocity bins is assumed to be completely mixed. Two simulations are shown for two different mass-cuts, $M_{\text{cut}} = 2.41 M_{\odot}$ (solid line with open circles), and $M_{\text{cut}} = 5.14 M_{\odot}$ (dashed-dotted line with open circles).

- d) The abundances of O, Mg, Al and Na hardly depend on the explosion energy and mass-cut, but interestingly Al and Na must be more overabundant than O and Mg in contrast with the observed abundances.

4.1.2. Aspherical SN explosion

The derived heliocentric radial velocity of $\sim -167.1 \text{ km s}^{-1}$ is much larger than the system kick ($\sim 50 \text{ km s}^{-1}$) gained from a spherically symmetric supernova explosion. Brandt et al. (1995) suggested the black hole in Nova Sco 94 could have formed in a two-stage process where the collapse first leads to the formation of a neutron star accompanied by a supernova kick, which subsequently converted into a black hole by fallback. Podsiadlowski et al. (2002) also investigated the expected abundances in the companion star after pollution of nucleosynthetic products in a non-spherically symmetric supernova. They found good fits to the observed abundances reported in Israelian et al. (1999). In their simulations they also took into account possible losses of mass of the He core progenitor in a stellar wind before the explosion and the pollution because of the capture of wind material. This allowed them to use He core progenitor with masses as high as $16 M_{\odot}$, hence reducing the matter ejected in the SN explosion and preventing from the disruption of the system.

We have also inspected an aspherical explosion model of a $16 M_{\odot}$ He core progenitor with an explosion energy of 10×10^{51} ergs from Maeda et al. (2002). We did not consider mass losses from the helium star via stellar winds and hence the greater amount of ejected matter only requires to capture roughly 10% of the matter ejected within the solid angle subtended by the secondary. We computed the expected abundances in the secondary star after pollution from the SN products assuming that the secondary star was located in the equatorial plane of the helium star before the explosion. In this case, the mass-cut varies from 2.41 to $5.14 M_{\odot}$ in steps of $\sim 0.6 M_{\odot}$. Fig. 13 shows the comparison of the observed abundances with the expected abundances in the secondary star after pollution from the SN ejecta. The error bars in Fig. 13 correspond to the total errors given in Table 4.

As in the spherical case we show two models and two different mass-cuts. The left panel reflects the composition of the material ejected in the equatorial plane while in the right panel we have considered complete lateral mixing (Podsiadlowski et al. 2002), i.e. the ejected matter is completely mixed within each velocity bin. Note that in the left panel we selected two close values of the mass-cut while in the right panel the whole dependence on the mass-cut is shown. The model with complete lateral mixing tends to enhance all the element abundances for each mass-cut. The analysis of the aspherical case provides the following conclusions:

- The aspherical model predicts too low abundances of S for any mass-cut unless complete lateral mixing is assumed.
- However, in the model with complete lateral mixing, in spite of the fact that Na abundance decreases until being almost marginally consistent with the observed value, the observed Al still remains too low in comparison with its expected abundance.
- Moreover, this model increases Ca, Ti, Fe and Ni abundances by a factor of 2–3 above the observed values.

A complete grid of models with a wide range of progenitor masses and explosion energies may be required to study in detail the abundance pattern of the secondary star in this system.

5. Conclusions

We have presented a VLT/UVES high resolution spectroscopy of the black hole binary Nova Sco 94. The individual spectra of the system allowed us to derive an orbital period of $P = 2.62120 \pm 0.00014$ days and a radial velocity semi-amplitude of the secondary star of $K_2 = 226.1 \pm 0.8 \text{ km s}^{-1}$. The implied updated mass function is $f(M) = 3.16 \pm 0.03 M_{\odot}$, consistent with previous values reported in the literature. The inspection of the high-quality averaged spectrum of the secondary star provides a rotational velocity of $v \sin i = 87^{+8}_{-4} \text{ km s}^{-1}$, and hence a binary mass ratio $q = 0.329 \pm 0.047$. The derived radial velocity,

$\gamma = -167.1 \pm 0.6 \text{ km s}^{-1}$, of the center of mass of the system disagrees, at the 3σ level, with previous studies.

We have performed a detailed chemical analysis of the secondary star. We applied a technique that provides a determination of the stellar parameters, taking into account any possible veiling from the accretion disc. We find $T_{\text{eff}} = 6100 \pm 200 \text{ K}$, $\log(g/\text{cm s}^2) = 3.7 \pm 0.2$, $[\text{Fe}/\text{H}] = -0.1 \pm 0.1$, and a disc veiling (defined as $F_{\text{disc}}/F_{\text{total}}$) of less than 10% at 5000 Å and decreasing toward longer wavelengths.

We have revised the chemical abundances of O, Mg, S, Si, Ti and Fe already reported in Israelian et al. (1999) and determined new element abundances of Na, Al, Ca, Ni and Li. The element abundances are typically higher than solar except for Fe, Ca and Ni, and in some cases significantly enhanced (e.g. O, Mg, S and Si). The abundance ratio of each element with respect to Fe were compared with those in stars with similar iron content of the solar neighbourhood. We confirm that O, Mg, Si, S and Na are considerably overabundant whereas Al, Ca, Ti and Ni appear to be practically consistent with the Galactic trends of these elements. We also report an upper limit of the Li abundance.

These chemical abundances strongly suggest that the secondary star captured part of the ejecta from a supernova explosion that originated the black hole in Nova Sco 94. We have compared these element abundances with element yields from a variety of SN explosion models for different energies and geometries. An spherically symmetric explosion model of 30 M_{\odot} progenitor (with a He core of 8.5 M_{\odot}) suggests a mass-cut between 2–3.5 M_{\odot} for kinetic energies $(1 - 20) \times 10^{51}$ ergs, based on the relatively low abundances of Ca, Ti, Ni and Fe. The greatly enhanced abundances of Si and specially S in the secondary star favours higher kinetic energies and therefore a hypernova explosion, and requires efficient mixing processes between the fallback matter and the ejecta.

The kinematic properties of the system suggest that a natal kick was imparted to the compact object at birth due to an asymmetry in the neutrino emission if a neutron star formed first, and/or an asymmetric mass ejection. We have also inspected a non-spherically symmetric SN explosion model with a 16 M_{\odot} He core progenitor, but this model provides unacceptable fits to the observed abundances because they require complete lateral mixing and produced too high abundances of Ca, Ti, Fe and Ni. We have also found relatively low Na and Al abundances which cannot be explained with the current spherical and aspherical SN models.

Acknowledgements. We are grateful to Hideyuki Umeda, Ken'ichi Nomoto, and Nozomu Tominaga for kindly sending us their spherically symmetric explosion models and several programs for our model computations. We also thank Keiichi Maeda for providing us with his aspherical explosion models, and for helpful discussions. We would like to thank Martin A. Bitner and Edward L. Robinson for kindly sending us the code `LNBROB`. We are grateful to Tom Marsh for the use of the MOLLY analysis package. This work has made use of the VALD database and IRAF facilities. J. I. acknowledges support from the EU contract MEXT-CT-2004-014265 (CIFIST). This work has been also funded by the Spanish Ministry project AYA2005-05149.

References

Abia, C., & Mashonkina, L. 2004, *MNRAS*, 350, 1127
 Allende Prieto, C., Barklem, P. S., Lambert, D. L., & Cunha, K. 2004, *A&A*, 53, 181
 Al-Naimiy, H. M. 1978, *Ap&SS*, 420, 183
 Andrievsky, S. M., Chernyshova, I. V., Usenko, I. A., Kovtyukh, V. V., Panchuk, V. E., & Galazutdinov, G. A. 1995, *PASP*, 107, 219
 Asplund, M. 2005, *ARA&A*, 43, 481
 Baily, C. D., Orosz, J. A., McClintock, J. E., & Remillard, R. A. 1995, *Nature*, 378, 157
 Balachandran, S. 1991, *Mem. Soc. Astron. Italiana*, 62, 33
 Baumüller, D., & Gehren, T. 1996, *A&A*, 307, 961
 Baumüller, D., & Gehren, T. 1997, *A&A*, 325, 1088

Baumüller, D., Butler, K., & Gehren, T. 1998, *A&A*, 338, 637
 Beer, M. E., & Podsiadlowski, Ph. 2002, *MNRAS*, 331, 351
 Bitner, M. A., & Robinson, E. L. 2006, *AJ*, 131, 1712
 Boesgaard, A. M., & Tripicco, M. J. 1986, *ApJ*, 302, L49
 Boesgaard, A. M., & Tripicco, M. J. 1987, *ApJ*, 313, 389
 Brandt, W. N., Podsiadlowski, Ph., & Sigurdsson, S. 1995, *MNRAS*, 277, L35
 Brown, G. E., Lee, C.-H., Wijers, R. A. M. J., Lee, H. K., Israelian, G., & Bethe, H. A. 2000, *NewA*, 5, 191
 Buxton, M., & Vennes, S. 2001, *Publ. Astron. Soc. Aust.*, 18, 91
 Castelli, F., & Kurucz, R. L. 2003, *IAU Symposium*, 210, 20P
 Ecuivillon, A., Israelian, G., Santos, N. C., Mayor, M., Villar, V., & Bihain, G. 2004, *A&A*, 426, 619
 Ecuivillon, A., Israelian, G., Santos, N. C., Shchukina, N. G., Mayor, M., & Rebolo, R. 2006, *A&A*, 445, 633
 Foellmi, C., Depagne, E., Dall, T. H., & Mirabel, I. F. 2006, *A&A*, 457, 249
 Foellmi, C., Dall, T. H., & Depagne, E. 2007, *A&A*, 464, L61
 Galazutdinov, G. A., Musaev, F. A., Krelowski, J., & Walker, G. A. H. 2000, *PASP*, 112, 648
 Gilli, G., Israelian, G., Ecuivillon, A., Santos, N. C., & Mayor, M. 2006, *A&A*, 449, 723.
 González Hernández, J. I., Rebolo, R., Israelian, G., Casares, J., Maeder, A., & Meynet, G. 2004, *ApJ*, 609, 988
 González Hernández, J. I., Rebolo, R., Israelian, G., Casares, J., Maeda, K., Bonifacio, P., & Molero, P. 2005, *ApJ*, 630, 495
 González Hernández, J. I., Rebolo, R., Israelian, G., Harlaftis, E. T., Filippenko, A. V., & Chornock, R. 2006, *ApJ*, 644, L49
 Grevesse, N., Noels, A., & Sauval, A. J. 1996, *The sixth annual October Astrophysics Conference*, ASP Conf. Ser. 99, 117
 van der Hooft, F., Heemskerk, M. H. M., Alberts, F., & van Paradijs, J. 1998, *A&A*, 329, 538
 Israelian, G., Rebolo, R., Basri, G., Casares, J., & Martín, E. L. 1999, *Nature*, 401, 142
 Kifonidis, K., Plewa, T., Janka, H.-Th., & Miller, E. 2000, *A&A*, 531, L123
 Kurucz, R. L. ATLAS9 Stellar Atmospheres Programs and 2 km s⁻¹ Grid. (CD-ROM, Smithsonian Astrophysical Observatory, Cambridge, 1993).
 Kurucz, R. L., Furenlid, I., Brault, J., & Testerman, L. 1984, *Solar Flux Atlas from 296 to 1300 nm*, NAOA Atlas 1 (Cambridge: Harvard Univ. Press)
 Maeda, K., Nakamura, T., Nomoto, K., Mazzali, P. A., Patat, F., & Hachisu, I. 2002, *ApJ*, 565, 405
 Marsh, T. R., Robinson, E. L., & Wood, J. H. 1994, *MNRAS*, 266, 137
 Mashonkina, L., Korn, A. J., & Przybilla, N. 2007, *A&A*, 461, 261
 Mirabel, I. F., Mignani, R., Rodrigues, I., Combi, J. A., Rodríguez, L. F., & Guglielmetti, F. 2002, *A&A*, 395, 595
 Orosz, J. A., & Baily, C. D. 1997, *ApJ*, 477, 876
 Pavlenko, Ya. V., & Magazzù, A. 1996, *A&A*, 311, 961
 Piskunov, N. E., Kupka, F., Ryabchikova, T. A., Weiss, W. W., & Jeffery, C. S. 1995, *A&AS*, 112, 525
 Podsiadlowski, P., Nomoto, K., Maeda, K., Nakamura, T., Mazzali, P., & Schmidt, B. 2002, *ApJ*, 567, 491
 Sbordone, L., Bonifacio, P., Castelli, F., & Kurucz, R. L., 2004, *MSAIS*, 5, 93
 Shimanskaya, N. N., Mashonkina, L. I., & Sakhibullin, N. A. 2000, *Astron. Rep.*, 44, 530
 Shchukina, N. G. 1987, *Kinemat. Phys. Celest. Bodies*, 3, 36
 Shchukina, N. G., & Trujillo Bueno, J. 2001, *ApJ*, 550, 970
 Shahbaz, T., van der Hooft, F., Casares, J., Charles, P. A., & van Paradijs, J. 1999, *MNRAS*, 306, 89
 Shahbaz, T. 2003, *MNRAS*, 339, 1031
 Sneden, C. 1973, PhD Dissertation (Univ. of Texas at Austin)
 Takada-Hidai, M., Takeda, Y., Sato, S. et al. 2002, *ApJ*, 573, 614
 Takeda, Y., Hashimoto, O., Taguchi, H. et al. 2005, *PASJ*, 57, 751
 Takeda, Y., & Honda, S. 2005, *PASJ*, 57, 65
 Tominaga, N., Umeda, H., & Nomoto, K. 2007, *ApJ*, 660, 516
 Umeda, H., & Nomoto, K. 2002, *ApJ*, 565, 385
 Umeda, H., & Nomoto, K. 2005, *ApJ*, 619, 427
 Wedemeyer, S. 2001, *A&A*, 373, 998
 Zhang, S. N., Wilson, C. A., Harmon, B. A., Fishman, G. J., Wilson, R. B. et al. 1994, *IAU Circ.*, 6046
 Zhao, G., Butler, K., & Gehren, T. 1998, *A&A*, 333, 219
 Zhao, G., & Gehren, T. 2000, *A&A*, 362, 1077